Crystal and Solution Studies Reveal That the Transcriptional Regulator AcnR of *Corynebacterium glutamicum* Is Regulated by Citrate-Mg^{2+} Binding to a Non-canonical Pocket[S]

Javier García-Nafría[‡1,2], **Meike Baumgart**[§1], **Johan P. Turkenburg**[‡], **Anthony J. Wilkinson**[‡], **Michael Bott**[§3], and **Keith S. Wilson**[‡4]

From the [‡]York Structural Biology Laboratory, Department of Chemistry, University of York, York YO10 5DD, United Kingdom and the [§]Institute of Bio- and Geosciences, IBG-1: Biotechnology, Wilhelm-Johnen-Strasse, Forschungszentrum Jülich, 52425 Jülich, Germany

Background: AcnR is an aconitase repressor in the biotechnologically important bacterium *Corynebacterium glutamicum*.
Results: Citrate-Mg^{2+} occupies a non-canonical ligand site and lowers the DNA affinity of AcnR.
Conclusion: AcnR is regulated by citrate-Mg^{2+} through a non-canonical binding site.
Significance: AcnR is the first TetR member with potentially two independent ligand binding sites. Identification of citrate-Mg^{2+} as a ligand is crucial for understanding its physiological role.

Corynebacterium glutamicum **is an important industrial bacterium as well as a model organism for the order Corynebacteriales, whose citric acid cycle occupies a central position in energy and precursor supply. Expression of aconitase, which isomerizes citrate into isocitrate, is controlled by several transcriptional regulators, including the dimeric aconitase repressor AcnR, assigned by sequence identity to the TetR family. We report the structures of AcnR in two crystal forms together with ligand binding experiments and *in vivo* studies. First, there is a citrate-Mg^{2+} moiety bound in both forms, not in the canonical TetR ligand binding site but rather in a second pocket more distant from the DNA binding domain. Second, the citrate-Mg^{2+} binds with a K_D of 6 mM, within the range of physiological significance. Third, citrate-Mg^{2+} lowers the affinity of AcnR for its target DNA *in vitro*. Fourth, analyses of several AcnR point mutations provide evidence for the possible involvement of the corresponding residues in ligand binding, DNA binding, and signal transfer. AcnR derivatives defective in citrate-Mg^{2+} binding severely inhibit growth of *C. glutamicum* on citrate. Finally, the structures do have a pocket corresponding to the canonical tetracycline site, and although we have not identified a ligand that binds there, comparison of the two crystal forms suggests differences in the region of the canonical pocket that may indicate a biological significance.**

Corynebacterium glutamicum is a non-pathogenic, predominantly aerobic Gram-positive soil bacterium that can excrete glutamate (1) and is used industrially for the large scale production of amino acids, in particular L-glutamate (about 2.16 million tons/year) and L-lysine (about 1.48 million tons/year). Because the world market for amino acids is continuously increasing, there are ongoing efforts to improve production strains and processes (2). *C. glutamicum* has also gained interest as a model organism for the order Corynebacteriales, which includes the human pathogens *Corynebacterium diphtheriae* and *Mycobacterium tuberculosis*. A wealth of knowledge on *C. glutamicum* has been summarized in a handbook (3) and two monographs (4, 5). The citric acid (tricarboxylic acid, TCA)[5] cycle of *C. glutamicum* has been studied intensively because of its importance in energy metabolism and in the production of the amino acid precursors oxaloacetate and 2-oxoglutarate (6, 7). Because substrate carbon is lost as carbon dioxide in the TCA cycle, regulation of the carbon flux through this cycle is of special interest for biotechnological production processes. AcnR was identified as the first transcriptional regulator of a TCA cycle enzyme in *C. glutamicum* and functions as a repressor of *acn*, which is to date its only known target gene (8). AcnR is conserved in all corynebacteria and mycobacteria and binds as a dimer to an imperfect inverted repeat (5'-CAGAACGCT-TGTACTG-3') located within the −10/−35 region of the *acn* promoter. Comparison with the *acn* promoter region of other species identified a consensus binding motif (CAGNACnnnc-GTACTG). An *acnR* deletion mutant grows slightly faster than the wild type on glucose or acetate minimal medium and has an increased aconitase activity (5.3-fold higher on glucose and 1.9-fold higher on acetate). When cultivated in a medium with a low iron content, overproduction of aconitase in the *acnR* mutant causes iron limitation (8).

Aconitase is the second enzyme in the TCA cycle and catalyzes the stereospecific isomerization of citrate to isocitrate via *cis*-aconitate (9, 10) and is also involved in the glyoxylate and

---

the methylcitrate cycles (6). In the latter, it catalyzes the conversion of 2-methylaconitate to 2-methylisocitrate. In contrast to organisms such as *Escherichia coli* (11), *C. glutamicum* possesses only a single aconitase containing a [4Fe-4S] cluster, which is crucial for catalytic activity and which is highly oxygen-sensitive (10, 12). Previous studies revealed that the flux through the TCA cycle (13) as well as the aconitase activity differs significantly in cells grown on different carbon sources (aconitase activity on glucose, 0.20 ± 0.05 unit mg^{-1}; propionate, 0.47 ± 0.13 unit mg^{-1}; citrate, 0.53 ± 0.08 unit mg^{-1}; acetate, 0.82 ± 0.08 unit mg^{-1}), suggesting that the aconitase reaction might represent a rate-limiting step in this cycle (8). In addition, an aconitase deletion mutant faces strong selection pressure to lose citrate synthase activity, probably caused by high intracellular citrate concentrations (12). This explains the tight regulation of *acn* in *C. glutamicum* by at least four different regulators, AcnR, RipA (14), RamA (15), and GlxR (16). RipA is part of the iron homeostasis control system and represses transcription of *acn* under iron starvation conditions (17). Activation of *acn* transcription by RamA during growth on acetate is probably required to allow for an increased flux through the TCA cycle on this substrate (13, 18). The cAMP sensor GlxR is a global transcriptional regulator that controls at least 150 genes in a broad functional context (19, 20) with a function in global coordination of metabolism.

AcnR belongs to the TetR family of dimeric transcriptional regulators (21), whose members contain an N-terminal DNA-binding domain (DBD) and a C-terminal dimerization and ligand-binding domain (LBD) (22). Although there are large differences in the LBD, which allow for the response to different ligands, the sequence and structure of the DBD are highly conserved. Although several three-dimensional structures of TetR-type regulators have been determined, there are only four examples where all three functional forms (free protein, complex with operator, and complex with effector) are known: *E. coli* TetR (23, 24), *Staphylococcus aureus* QacR (25, 26), *C. glutamicum* CgmR (27, 28), and *Streptomyces antibioticus* SimR (29, 30). It is assumed that binding of a ligand to the LBD causes AcnR to be released from the DNA, allowing the expression of the aconitase gene. Although a large number of putative effector compounds were tested, no ligand of AcnR was identified in previous studies (8).

Current structures of TetR family proteins reveal the evolution of two different types of binding pockets. In the first, the two symmetric subunits contribute to form a single large pocket, whereas the second contains two independent symmetrically located smaller pockets, one within each subunit. This latter site, where tetracycline binds in TetR, we will refer to as the canonical site. The nature of the ligand is critical for understanding the regulatory mechanism and physiological function of AcnR, and we initiated structural studies with the aim of establishing its identity (31). Here, we present crystal structures of AcnR showing that citrate-Mg^{2+} binds to a quite different non-canonical pocket. The affinity of the citrate-Mg^{2+}, measured using surface plasmon resonance, is shown to be within the biologically relevant range. The presence of Mg^{2+} is strictly required for citrate binding to AcnR, which significantly lowers the affinity of AcnR for DNA. Although AcnR does contain a

bigger canonical pocket similar to that of the tetracycline site in TetR, this site is empty in our structures. Finally, we relate the properties of a set of AcnR variants to our structural and biochemical studies.

EXPERIMENTAL PROCEDURES

Bacterial Strains, Plasmids, and Growth Media—All strains and plasmids used are listed in supplemental Table S1. For plasmid-harboring strains, the medium was supplemented with 25 mg $liter^{-1}$ (*C. glutamicum*) or 50 mg $liter^{-1}$ (*E. coli*) kanamycin. For induction of target genes cloned into the expression plasmid pEKEx2 or pAN6, isopropyl-β-D-thiogalactopyranoside was used in concentrations as specified. For cloning purposes, *E. coli* DH5α was used and grown at 37 °C in lysogeny broth (LB) (32).

Recombinant DNA—The enzymes for recombinant DNA work were obtained from New England Biolabs (Frankfurt, Germany) or Fermentas (St. Leon-Rot, Germany). The oligonucleotides were obtained from Operon (Cologne, Germany) and are listed in supplemental Table S2. Routine methods such as PCR, restriction, and ligation were performed using standard protocols (32). Chromosomal DNA of *C. glutamicum* was prepared as described previously (33). *E. coli* plasmids were isolated using the QIAprep spin miniprep kit (Qiagen, Hilden, Germany). *E. coli* was transformed using the RbCl method (34).

The plasmid pET-TEV-AcnR was constructed as follows. The AcnR coding region was amplified by PCR using the oligonucleotides acnR-Krist-for-NdeI and acnR-Krist-rev-XhoI and chromosomal DNA of *C. glutamicum* ATCC 13032 as template. After digestion with NdeI and XhoI, the PCR product was cloned into the expression vector pET-TEV cut with the same restriction enzymes. The pET-TEV-AcnR-encoded AcnR derivative contained 29 additional N-terminal amino acids (MGSSHHHHHHHHHHHDYDIPTTENLYFQGH), of which, after cleavage with tobacco etch virus (TEV) protease, only three additional amino acids (GHM) remained at the N terminus.

The plasmid pET-TEV-MtAcnR was constructed according to pET-TEV-AcnR, using the oligonucleotides Mt_AcnR_NdeI_fw and Mt_AcnR_XhoI_rv and chromosomal DNA of *M. tuberculosis* strain H37rv as template. For the plasmid pMal-c-MtAcnR, the *acnR* gene of *M. tuberculosis* and the codons of the TEV cleavage site were amplified using the oligonucleotides TEV-site-Eco-fw and Mt_AcnR_XbaI_rv and the plasmid pET-TEV-MtAcnR as template. After digestion with EcoRI and XbaI, the PCR product was cloned into the plasmid pMal-c cut with the same restriction enzymes. The MtAcnR derivative encoded by this plasmid contains the maltose-binding protein of *E. coli* at its N terminus, which can be cleaved off by TEV protease as described above.

Site-directed Mutagenesis—Plasmids which code for *C. glutamicum* AcnR variants with single amino acid exchanges (C23A, K43A, K55A, E65A, D66A, R69A, M70A, M86A, R92A, W95A, R99A, K104A, D119A, R130A, R141A, D143A, D158A, E181A, and R185A) were constructed with the QuikChange XL site-directed mutagenesis kit (Stratagene) using the plasmids pEKEx2-acnR-C-Strep or pET-TEV-AcnR as template and the oligonucleotides listed in supplemental Table S2. pEKEx2-

acnR-C-Strep is an *E. coli/C. glutamicum* shuttle plasmid and allows overproduction of an AcnR derivative containing 10 additional C-terminal amino acids (LEWSHPQFEK), including a *Strep*Tag-II sequence. The *Strep*Tag-II allows for affinity purification of AcnR by StrepTactin affinity chromatography (35).

Overproduction and Purification of AcnR and Mutated Variants by Nickel Chelate Affinity Chromatography—This was carried out as described earlier (31). In contrast to our earlier studies (8), tag-free AcnR was used here for all experiments because (i) AcnR proved to be more stable over longer time periods without the tag; (ii) although the tag did not interfere with DNA binding, it might influence ligand binding to AcnR; and (iii) crystallization trials with His-tagged AcnR were not successful.

Purification of AcnR and Variants by StrepTactin Affinity Chromatography—Overexpression and purification were performed as described previously (36). Subsequently, gel filtration was performed with a Superdex™ 200 10/300 GL column connected to an Äkta™ FPLC system using the same buffer as for the His tag derivative. The mutant derivatives of AcnR were concentrated to $0.07–0.27$ mg ml^{-1} and stored frozen as for the wild-type protein.

Purification of MtAcnR by Maltose-binding Protein Affinity Chromatography—Overexpression using the plasmid pMal-c-MtAcnR was performed as described for pET-TEV-AcnR except that after induction, the cells were further cultivated at 15 °C overnight. The cells from 50 ml of culture were resuspended in 4 ml of buffer M (50 mM Tris-HCl, pH 8.0, 500 mM NaCl)/g of cells, and protease inhibitor was added (10 μl each of 100 mM phenylmethanesulfonyl fluoride and 100 mM diisopropyl fluorophosphates per ml of cell suspension). Cell disruption and cell extract preparation were performed as described above. An amylose resin (New England Biolabs) column with a bed volume of 5 ml was equilibrated with buffer M. The cell extract was applied onto the column, followed by washing with 20 ml of buffer M. Elution was performed with buffer M additionally containing 10 mM maltose.

Crystallization, Data Collection, and Structure Solution—AcnR was crystallized as described previously (31). In brief, crystals were obtained with protein concentrated at 26.5 mg ml^{-1} incubated with 5 mM sodium citrate and 5 mM MgCl$_2$ and set up in $300 + 300$-μl drops of 1 M ammonium phosphate, 100 mM sodium citrate, pH 4, and optimized. Data were collected on two native crystals, one on beamline I02 at the Diamond Light Source and another on beamline ID-29 at the European Synchrotron Radiation Facility (ESRF). Integration and scaling of the images with iMOSFLM (37, 38) and SCALA (39) revealed that there were two crystal forms, both in Laue group Pmmm, which differ by a doubling of the *c* axis in Form II. Subsequent calculations were carried out with programs from the CCP4 suite (40) unless otherwise indicated. Form I is in space group P2$_1$2$_1$2 with data to 1.9 Å spacing with one protomer per asymmetric unit, and Form II is in P2$_1$2$_1$2$_1$ with data to 1.6 Å with a dimer in the asymmetric unit. The two independent protomers in the Form II crystal have significant conformational differences in the canonical pocket (see below).

A heavy atom derivative was obtained (31) using 2 mM KAu(CN)$_2$. Data were collected to 2.55 Å resolution on beam-

line ID14-1 at the ESRF and processed using HKL2000 (41). The derivative was isomorphous with the Form I native. The structure was solved by SAD with SHELXC/D/E (42), and automatic model building with BUCCANEER (43) gave 90% of the residues. Rebuilding and refinement were done with COOT (44) and REFMAC (45) to final $R_{\text{work}}/R_{\text{free}}$ of 19.4/26.3%.

The resulting model was used for the refinement of Form I and for molecular replacement using PHASER (46) to solve the native Form II. The protein was modeled for residues $\sim 11–187$, with the last visible residue at each end varying slightly between the three crystals. The Form I and II native models were refined to $R_{\text{work}}/R_{\text{free}}$ of 19.4/24.6% and 14.1/20.5%, respectively. For all three structures, all residues are in the allowed region of the Ramachandran plot (47). A summary of the data and refinement statistics is shown in Table 1.

Electrophoretic Mobility Shift Assay (EMSA)—The binding of AcnR or variants to the *acn* promoter of *C. glutamicum* was tested. A 340-bp DNA fragment covering the *acn* promoter region was amplified by PCR using chromosomal DNA of the *C. glutamicum* ATCC 13032 strain as template and the oligonucleotide pair acn-Prom-5-for/acn-Prom-3-rev for unlabeled DNA and Cy3-acn-Prom-5-for/Cy3-acn-Prom-3-rev (343 bp) for Cy3-labeled DNA. The promoter region of cg1848, which served as nonspecific DNA for the competition experiment, was amplified using the oligonucleotide pair NCgl1580-for/NCgl1580-rev and chromosomal DNA of the ATCC 13032 strain as template. For the EMSAs with MtAcnR, the *M. tuberculosis* aconitase promoter region was amplified using the oligonucleotides Mt_Acn_Prom_fw and Mt_Acn_Prom_rv and chromosomal DNA of *M. tuberculosis* strain H37rv as template. In a second PCR using the oligonucleotides Cy3-acn-Prom-5-for and Mt_Acn_Prom_rv and the product from the first PCR as template, the DNA was labeled with Cy3 for detection.

The products were purified with a PCR purification kit (Qiagen, Hilden, Germany) and eluted in EB buffer. Purified AcnR protein was incubated with the DNA fragment in a total volume of 20 μl. 9 ng of the Cy3-labeled DNA fragment corresponding to a final concentration of 2 nM was used for the EMSAs. Unless otherwise stated, the binding buffer contained 10 mM Tris-HCl, pH 7.5, 50 mM NaCl, 5% (v/v) glycerol, and 0.005% Triton X-100. The reaction mixtures were incubated at room temperature for 20 min and then loaded onto 10% native polyacrylamide gels.

When putative effectors were tested, AcnR was first incubated with the compound for 20 min at room temperature, followed by the addition of the DNA and a further 20-min incubation. Before loading onto the gel, 4 μl of loading buffer (0.01% (w/v) xylene cyanol blue, 0.01% (w/v) bromphenol blue, 20% (v/v) glycerol, 10% (v/v) 10× TBE (890 mM Tris base, 890 mM boric acid, 20 mM EDTA)) was added to each sample. Electrophoresis was performed on ice at 180 V for 1.5 h using 1× TBE. The EMSAs with citrate-Mg^{2+} were performed with loading and running buffer lacking EDTA.

The gels were subsequently scanned using a Typhoon Trio™ scanner (GE Healthcare). For determination of the apparent K_D values, the fluorescence intensity of the bands corresponding to unbound and protein-bound DNA was quantified using

TABLE 1

Data collection and refinement statistics

Values in parenthesis correspond to the high resolution shell.

	Au derivative	Native Form I	Native Form II
Data collection			
Source	ESRF	ESRF	Diamond Light Source
Beamline	ID14–1	ID-29	I02
Wavelength (Å)	0.9334	1.0032	0.9795
Space group	$P2_12_12$	$P2_12_12$	$P2_12_12_1$
Cell dimensions a, b, c (Å)	34.14, 72.88, 73.25	34.64, 72.73, 73.20	34.21, 72.79, 145.57
Resolution (Å)	2.54 (2.58-2.54)	1.9 (2.00-1.90)	1.65 (1.74-1.65)
R_{merge}	0.073 (0.149)	0.137 (0.658)	0.082 (0.436)
$I/\sigma I$	47.9 (21.9)	10.0 (3.6)	9.4 (2.7)
Completeness (%)	100 (100)	99.3 (99.9)	99.6 (99.2)
Redundancy	8.8 (8.4)	6.0 (6.2)	4.5 (4.5)
Refinement			
No. of unique reflections	6461	14,286	44,662
R_{work}/R_{free}	19.8/26.3	19.4/24.6	14.15/20.48
Protein residues	176	174	354
Residues modeled	11-186	13-186	A, 11-186; B, 11-187
Ligand/ion	4	2	9
Water	49	102	353
B-factors (Å^2)			
Protein	21.5	27.9	20.8
Ligand/ion	32.2	23.0	22.8
Water	24.5	37.8	37.4
r.m.s. deviations			
Bond lengths (Å)	0.016	0.019	0.021
Bond angles (degrees)	1.355	1.956	1.620
Ramachadran plot (%)			
Preferred regions	97.70	98.81	97.89
Allowed regions	2.3	1.19	2.11
Outliers	0	0	0
Protein Data Bank codes	4AC6	4AF5	4ACI

ImageQuant software (GE Healthcare), followed by calculation of the percentage of bound DNA. These values were plotted against the AcnR concentration in $\log_{10}$ scale, and a sigmoidal fit was performed using the Origin 7 software (OriginLab Corp., Northampton, MA), taking into account the *error bars* as well as 0 and 100% shifted DNA as asymptotes. The turning point of the curve was defined as the apparent K_D value.

Surface Plasmon Resonance—Experiments were conducted using a Biacore T200 (GE Healthcare). Purified AcnR was immobilized through standard amine coupling methods to a CM5 S-series sensor chip with the protein in running buffer (20 mM Tris-HCl, pH 7.4, 50 mM NaCl, 0.001% Tween 20). The final amount of protein on the chip accounted for ~4900 RU, allowing a theoretical maximum signal of ~44 RU for citrate alone with a 1:1 binding stoichiometry with AcnR protomers. AcnR was titrated using 2-fold serial dilutions of citrate and citrate-Mg^{2+}, providing 12 data points with 40 mM being the highest concentration. All measurements were conducted at 25 °C. The binding profiles were fit globally to a 1:1 interaction model using the responses at equilibrium. The response data were processed with BIAevaluation software using a reference surface to correct for any bulk refractive index changes and blank injections for double referencing. The titration was repeated three times and showed consistent results.

Growth Experiments with Strains Containing Mutational Variants of AcnR—*C. glutamicum* Δ*acnR* was transformed with pEKEx2 plasmids encoding the native protein or one of the mutational variants under the control of the P$_{tac}$ (48). This promoter is leaky and leads to a low level expression of the desired protein in *C. glutamicum* without induction by isopropyl-β-D-thiogalactopyranoside. 5 ml of brain-heart infusion broth (Difco) was inoculated with a colony from a fresh brain-heart

infusion broth agar plate and incubated over 1 day at 30 °C and 170 rpm. Cells of this preculture were washed once in phosphate-buffered saline (PBS; 137 mM NaCl, 2.7 mM KCl, 4.3 mM Na_2HPO_4, 1.4 mM KH_2PO_4, pH 7.3) and used to inoculate the second preculture, consisting of 20 ml of CGXII minimal medium (49) supplemented with 3,4-dihydroxybenzoate (30 mg liter^{-1}) as iron chelator and glucose (111 mM) as carbon source. Cells from the second preculture were used to inoculate the main cultures to an A_{600} of 1 in 48-well FlowerPlates®, which were subsequently incubated at 30 °C, 95% humidity, and 1200 rpm in a BioLector® (m2p-labs, Baesweiler, Germany). The wells contained 750 μl of CGXII minimal medium with either glucose (111 mM) or citrate (50 mM sodium citrate plus 5 mM $CaCl_2$) as carbon source (50). Growth of the BioLector® cultures was monitored by measuring the back-scatter at 620 nm with gains of 10, 15, and 20, respectively. All growth media were supplemented with 25 mg liter^{-1} kanamycin.

RESULTS

Affinity and Specificity of the AcnR-Operator Interaction—EMSA experiments with AcnR and Cy3-labeled operator DNA (Fig. 1A) gave an apparent K_D of 7.7 ± 0.9 nM for the binding of dimeric AcnR to its operator by plotting the percentage of shifted DNA *versus* the AcnR concentration from five independent experiments. Binding of AcnR to Cy3-labeled operator DNA was inhibited by the addition of unlabeled operator DNA but not by the addition of a control DNA (468-bp fragment covering the promoter region of cg1848) (Fig. 1B). These results confirm the specificity of the AcnR-operator interaction.

Initial Search for the Effector of AcnR—Citrate was considered as a prime candidate but showed no effect or only a very weak effect on DNA binding even when added to the gel and

the running buffer (data not shown). An extensive set of metabolites and cofactors was subsequently tested, including *cis*-aconitate, isocitrate, 2-methylcitrate, 2-methyl-*cis*-aconitate, acetate, acetyl-CoA, fumarate, oxaloacetate, propionate, succinyl-CoA, glucose 6-phosphate, L-glutamate, L-glutamine, a combination of all 20 amino acids, ADP, AMP, ATP, NAD^+, NADH, $NADP^+$, or NADPH. However, none had an inhibitory effect on DNA binding under the chosen conditions.
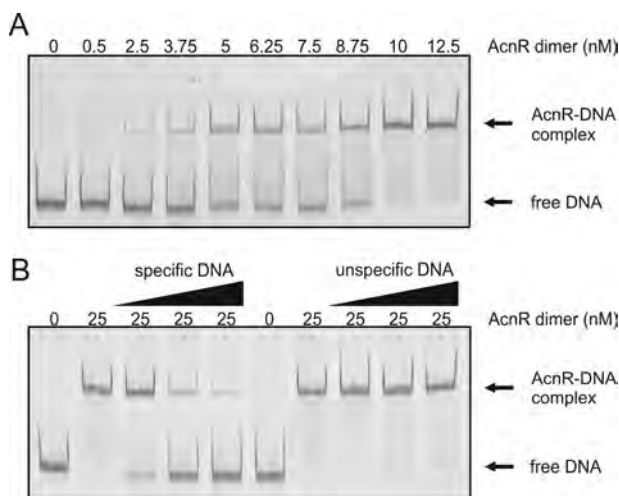

FIGURE 1. **Analysis of AcnR-DNA interaction by EMSAs.** *A*, determination of the apparent K_D for the binding of AcnR to its operator in the *acn* promoter. A 2 nM concentration of a Cy3-labeled DNA fragment covering the promoter region of *acn* was incubated with increasing concentrations of AcnR and analyzed as described under "Experimental Procedures." An apparent K_D of 7.7 ± 0.9 nM was determined for dimeric AcnR. *B*, competition experiment with specific and nonspecific DNA (unlabeled), 2 nM Cy3-labeled DNA of the *acn* promoter, and 25 nM AcnR dimer. Specific DNA was unlabeled *acn* promoter DNA (10 nM, 40 nM, 100 nM), and nonspecific DNA was a 468-bp fragment covering the promoter region of cg1848 (10, 40, and 100 nM).

Site-directed Mutagenesis—To identify residues involved in binding to DNA and to potential ligands, AcnR derivatives with single amino acid substitutions were constructed. For the first set (K43A, K55A, and K104A), gel filtration profiles showed that all three still formed dimers but that the ratio of aggregated to dimeric protein was significantly higher for K55A and K104A. EMSAs revealed that the DNA binding affinity was slightly reduced for K104A and almost completely abolished for K43A and K55A. A second set of variants with amino acid substitutions was created based on the structure and will be described below.

Structure of AcnR—We report the structure in two crystal forms, Form I with one subunit and Form II with a dimer in the asymmetric unit. The overall fold is similar in both forms.

Crystal Form I—The structures of the native protein and of the heavy atom derivative were solved in this form. The structure shows a typical dimeric TetR-type repressor, where each protomer is all-α with nine α-helices, arranged as a C-terminal dimerization LBD and an N-terminal DBD (Fig. 2) (reviewed in Ref. 22). The DBD is a three-helix bundle formed by α1, α2, and α3 stabilized by hydrophobic helix-to-helix contacts. Residues 1–11 (or 13 in the native protein) preceding α1 are disordered. α2 and α3 form the helix-turn-helix (HTH) motif responsible for DNA binding, α3 being the "recognition" helix responsible for the sequence-specific binding (21). Conserved TetR family residues in this motif form the hydrophobic core or are involved in DNA binding. The recognition helix is strictly conserved in the AcnR subfamily (Fig. 3), and it has a high positive electrostatic potential that contributes to DNA binding (Fig. 4*A*). It has been suggested that the N terminus of α4 could form part of the DBD because it moves together with it as a rigid unit in molec-
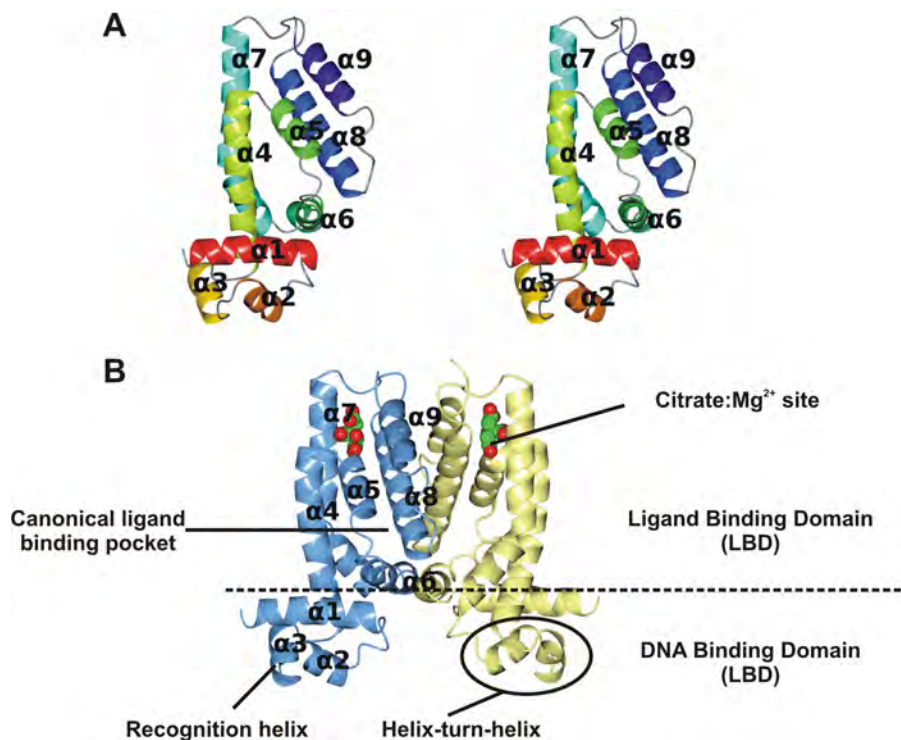
FIGURE 2. **The AcnR fold.** *A*, stereo view of the AcnR protomer *color-ramped* from *red* to *dark blue*. *B*, the AcnR dimer in Form I generated by the crystallographic 2-fold symmetry axis, *colored* by chain. In *B*, the citrate-Mg^{2+} is shown with a *space-filling representation*. Figs. 2–5 were created using CCP4mg (62).
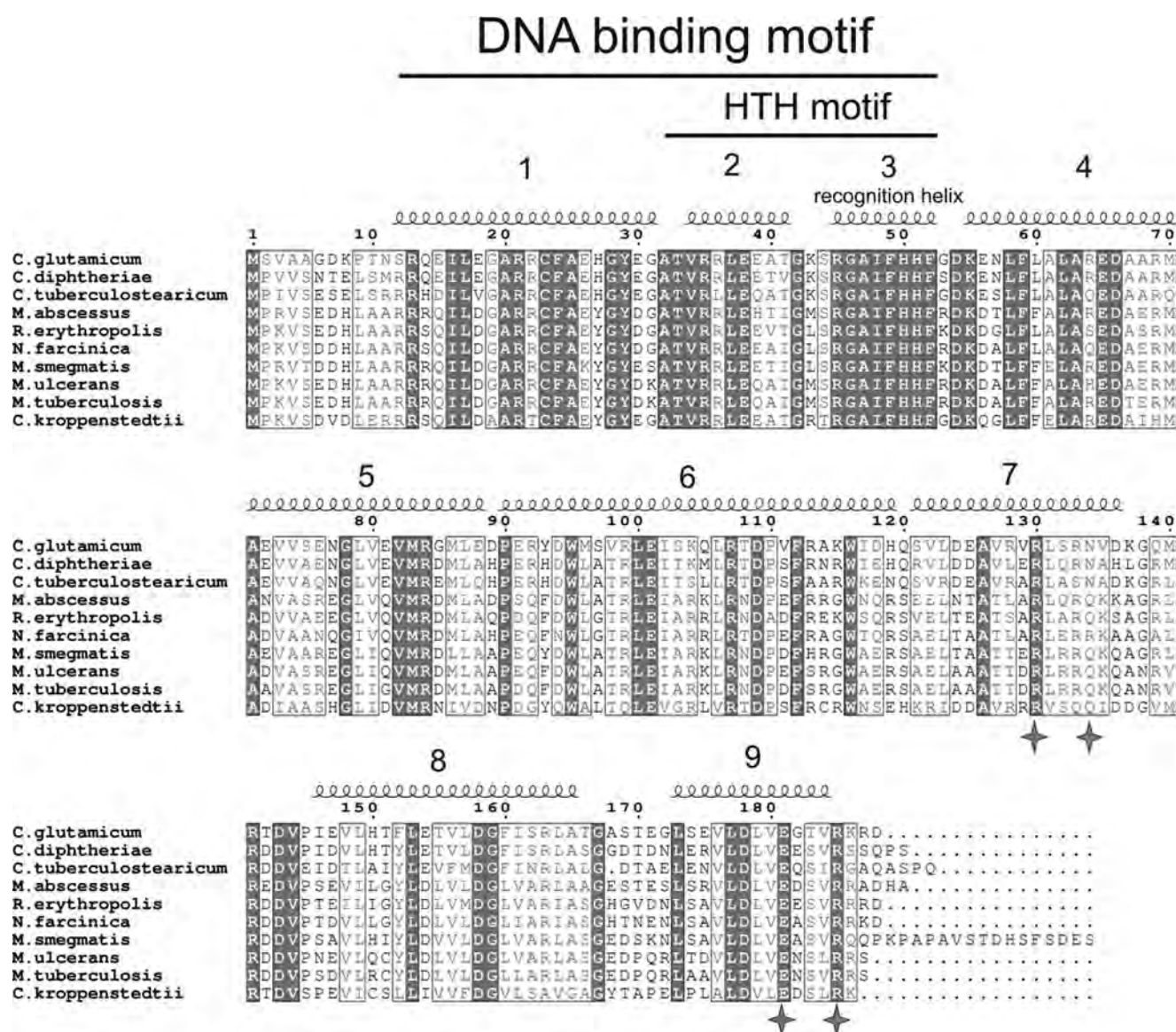
FIGURE 3. **Sequence alignment of AcnR homologues.** The conserved residues are *highlighted* in *dark gray*, whereas residues with similar physico-chemical properties are *boxed* in *white*. The residues hydrogen-bonding the citrate and magnesium ion are *highlighted* with a *star*.

ular dynamics simulations (51). $\alpha4$ also contains residues such as the conserved Lys-55 (AcnR numbering), which has been demonstrated to contribute a substantial part of the DNA binding energy in TetR (22). Because AcnR binds DNA at an inverted repeat, the distance between the two HTH motifs in the dimer should be ~34 Å when bound to two adjacent major grooves of DNA. The center-to-center distance in crystal Form I between the C_α of Phe-52 (at the center of the recognition helix) is somewhat longer, ~42 Å, but TetR-type regulators undergo significant conformational changes upon binding DNA, in addition to the significant changes between free and ligand-bound forms. Indeed, the distance is 40 Å in apo-TetR (52). The interactions between the DBD and LBD involve the C-terminal part of $\alpha1$ with $\alpha4$ and $\alpha6$ of the LBD and are conserved across the TetR family.

The LBD is responsible for dimerization and ligand binding and is formed by $\alpha4$–$\alpha9$. Although its sequence is poorly conserved (Figs. 3 and 4*B*), it has a common structural core in all

TetR-type regulators (22), involving a core triangle formed by three helices ($\alpha5$, $\alpha6$, and $\alpha7$) around which the other elements fold. This triangle is conserved in AcnR, with $\alpha7$ being significantly bent at Ser-121. $\alpha4$ runs parallel to $\alpha7$ at the front of the triangle contacting the DBD, whereas $\alpha8$ runs parallel to $\alpha5$ at the back of the triangle, and $\alpha9$ runs antiparallel to $\alpha8$. The dimerization interface is formed by a four-helix bundle made up of $\alpha8$ and $\alpha9$ positioned orthogonally to their counterparts in the other subunit, which buries a surface area of 1572 Å^2 calculated with PISA (53).

The Distal Pocket, a Citrate-Mg^{2+} Binding Site in an Unexpected Location—The structure revealed the presence of a citrate-Mg^{2+} moiety in both subunits of both crystal forms at a site not seen in previous TetR-type repressors (Fig. 5). Based on its distance to the DBD, this will be termed the distal (D) pocket in contrast to the expected canonical TetR site, termed the proximal (P) pocket. The small D pocket is formed by the loop between $\alpha4$ and $\alpha5$ and helices $\alpha7$, $\alpha8$, and $\alpha9$ and has a volume
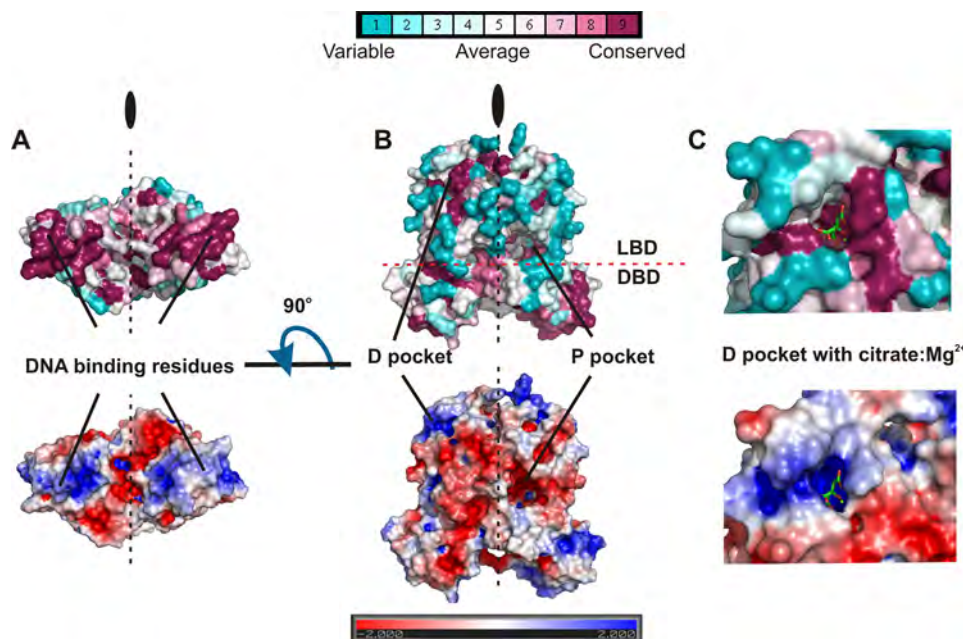
FIGURE 4. **Electrostatic potential and residue conservation in the AcnR DNA binding region (*A*) and pockets (*B* and *C*).** The protein is displayed as a *surface colored* by residue conservation (*top*) and electrostatic potential (*bottom*). Residue conservation ranges from fully conserved in *purple* to not conserved (*cyan*). Citrate (*green* carbons) is shown as cylinders in *C*.
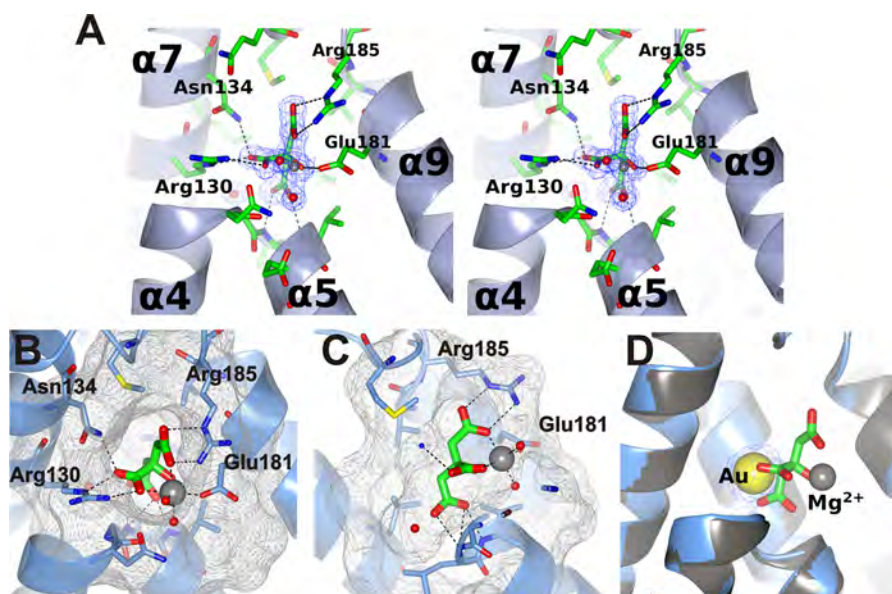

FIGURE 5. **The citrate binding distal pocket.** *A*, stereo view with the citrate and residues contacting the citrate or magnesium depicted as *cylinders*. The $2F_o - F_c$ map contoured at the 1σ level is shown for the citrate-Mg^{2+}. *B* and *C*, two views of the citrate-Mg^{2+} bound in the pocket of AcnR with the protein surface displayed to emphasize the shape of the pocket. *D*, superposition of the heavy atom derivative and native Form I structures. The $2F_o - F_c$ map at 1σ is shown for the gold ion. The gold in the derivative crystal displaces the citrate-Mg^{2+}.

of ~450 Å³. The ligand is positioned with its apolar carbon atoms pointing to the hydrophobic interior and the polar atoms facing the outer side of the pocket. The back of the pocket is formed by hydrophobic residues, including Leu-153, Leu-131, Leu-149, Val-184, and Met-140. The outer part is formed by polar residues (Asn-134, Arg-130, Glu-181, and Arg-185), which bind to the magnesium ion and the polar carboxyl groups of the citrate. The citrate oxygens form hydrogen bonds to the main chain amide groups from residues Leu-79 and Val-80 and to a water molecule. The magnesium ion is octahedrally coordinated by three oxygens of the citrate, two water molecules,

and the Glu-181 carboxyl oxygens (Fig. 5, *A–C*). All residues in the D pocket involved in contacts with the citrate-Mg^{2+} are conserved in other Corynebacteriales family members, including *M. tuberculosis* and *C. diphtheriae* (Figs. 3 and 4). This, together with the high specificity of the interactions and the fact that citrate is the substrate of aconitase, strongly suggests that the complex has biological relevance. Furthermore, the cavity has a high positive electrostatic potential, well suited to accommodate a molecule with negative charges, such as citrate (Fig. 4C).

In the derivative structure, four gold ions bind to each protomer. One displaces the citrate-Mg^{2+} bound in the native
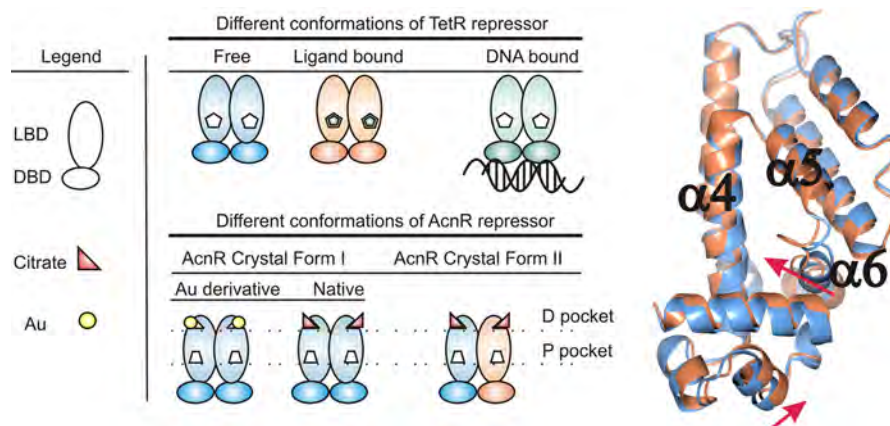
FIGURE 6. **Different states of the AcnR repressor.** *Left*, scheme of the different functional forms found in TetR repressor and those found in this work for AcnR**.** *Right*, comparison of the two independent AcnR protomers in the asymmetric unit (*blue* and *coral*) in crystal Form II. The two protomers are superposed, and the movements of $\alpha 6$ and the DBD relative to the LBD are evident.

structures (Fig. 5*D*). This displacement by the gold cyanide suggested only a moderate binding constant for the citrate-Mg^{2+}. The second gold is positioned in the DBD and the two others in the LBD.

Crystal Form II—There is a dimer in the asymmetric unit, made up of subunits A and B. Subunit A is very similar to the protomer seen in Form I, and superposition using SSM (54) showed an r.m.s. deviation over 177 equivalent C_α atoms of ~0.4 Å. In contrast, subunit B shows significant local differences with an overall r.m.s. deviation of equivalent C_α positions of ~1 Å from chain A or from Form I. The major differences are in the loop between $\alpha 5$ and $\alpha 6$ in the LBD and the relative position of the DBD with respect to the LBD (Fig. 6). The DBDs of both subunits superpose with an r.m.s. deviation of 0.5 Å, but the position relative to the LBD has changed by ~2 Å. The electron density for $\alpha 3$ in this subunit is weak, with the side chains of the aromatic residues being poorly defined. This could be due to disorder in the crystal but more likely reflects flexibility between the domains. The distance between the C_α of Phe-52 in the two subunits in this form is 42.6 Å, similar to that in Form I. The structures have been deposited in the Protein Data Bank with codes 4AF5 (Form I), 4AC6 (Form I Au derivative), and 4ACI (Form II).

A Possible Canonical P Pocket—There is a cavity in each subunit roughly corresponding to the canonical tetracycline binding site in TetR. In all of the AcnR subunits in native Forms I and II, this P pocket is empty. Although the P pocket is located at roughly the same place between the three core helices in the various TetR-type repressors for which structural data are available, the exact position of the ligands and size and shape of the pockets varies, reflecting the lack of sequence and hence local structure conservation. In Form I, the P pocket is large, with a volume of 1200 Å^3 calculated with CASTp (55). The entrance is on the opposite side to that of the D pocket and is formed by $\alpha 6 - \alpha 8$ and the loop between $\alpha 8'$ and $\alpha 9'$ from the other subunit. Residues in the entrance are mainly hydrophilic, whereas the inner part of the pocket is lined with hydrophobic residues. Electrostatic calculations with the PBEQ-solver server (56), which uses the CHARMM force field, shows that the cavity has a slightly negative charge (Fig. 4*B*). Sequence alignments

indicate that although Asp-66 and Trp-116 in site D are conserved (Fig. 3), the rest of the pocket lacks conserved residues.

In the LBD of Form 2, one protomer has part of $\alpha 6$ unwound and shifted toward the center of the canonical P pocket by 3 Å, closing it. This change in volume of the P pocket would be in keeping with the binding of a hypothetical ligand. The presence of two distinct binding sites per subunit would represent a new feature not seen before in TetR-type regulators and would imply a complex regulatory mechanism, but we should emphasize that we presently only have experimental evidence for the binding of citrate-Mg^{2+} and not of a second ligand.

Binding Affinity of Citrate-Mg^{2+}—Having observed the presence of citrate-Mg^{2+} in the D pocket with highly specific complementary interactions with conserved residues, we proceeded to measure the affinity constant using surface plasmon resonance. Maximum theoretical signals of ~44 and ~50 RU for citrate and citrate-Mg^{2+} were expected, respectively, for a 1:1 stoichiometry with an AcnR protomer. The results indicated clear binding of citrate-Mg^{2+} to AcnR in a 1:1 ratio with a signal of ~60 RU, whereas citrate alone did not show any measurable binding (even at 40 mM). A 1:1 Langmuir model gave a good fit based on the sum of the square residuals (χ^2), indicating a K_D of 6 mM (Fig. 7), within the range of biological significance. For *E. coli*, an intracellular citrate concentration of 2 mM has been reported (57), and higher concentrations are likely when, for example, aconitase activity is limiting. We conclude that citrate-Mg^{2+} is likely to contribute to AcnR regulation *in vivo*.

EMSA Studies with Citrate-Mg^{2+}—Because surface plasmon resonance measurements showed Mg^{2+} to be strictly required for binding of citrate, the EMSA studies were repeated using buffers lacking EDTA and revealed that the affinity of AcnR for DNA is reduced when both Mg^{2+} and citrate are present (Fig. 8*A*). Fig. 8*B* shows the reversibility of the citrate-Mg^{2+} effect upon DNA binding for removal of Mg^{2+} with EDTA. In addition, citrate-Ca^{2+} was tested but did not change the DNA binding affinity of AcnR (results not shown).

The Mutated AcnR Variants—A number of conserved charged residues were mutated to alanine to probe their functional relevance. Several of these exchanges were made in
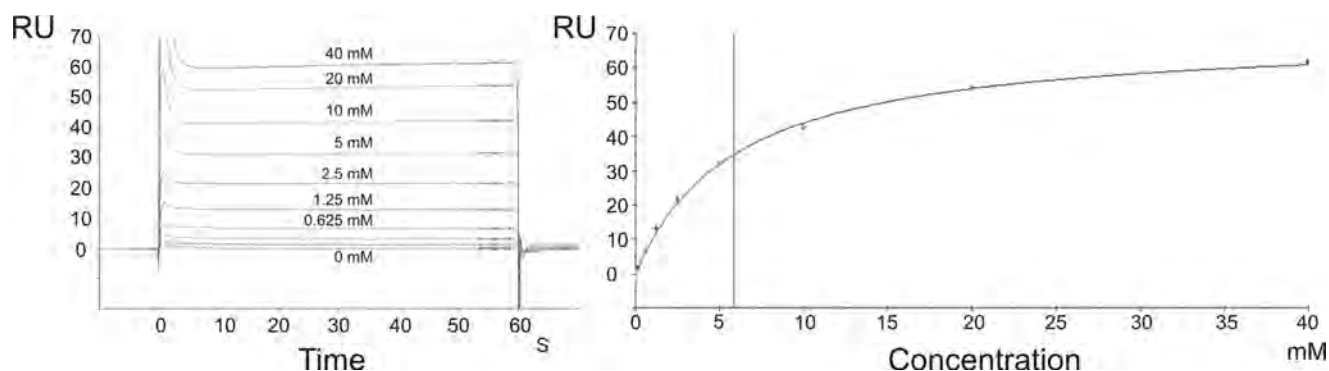
FIGURE 7. **Surface plasmon resonance titration of citrate-Mg^{2+} over AcnR.** *Left*, sensorgram showing responses at the different ligand concentrations. *Right*, 1:1 ratio Langmuir curve fitted to the resulting responses.
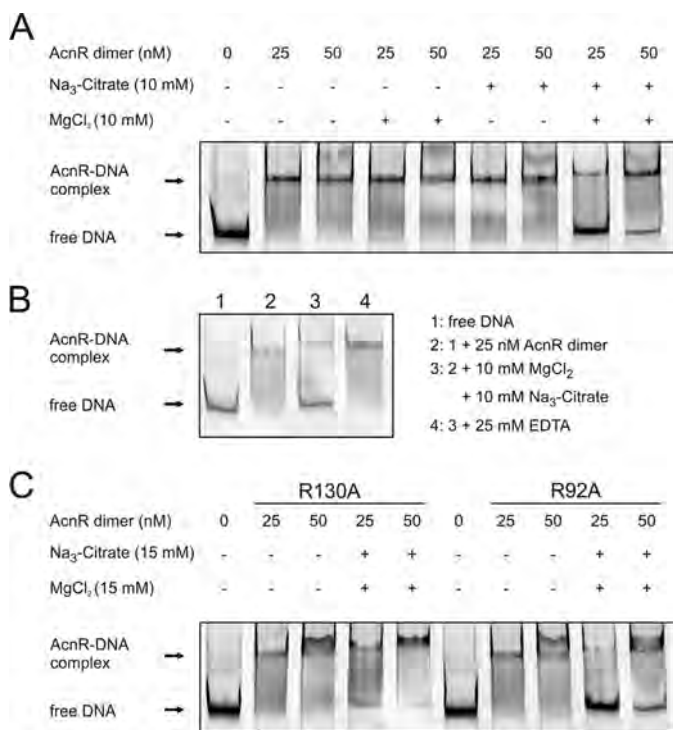

FIGURE 8. **Bandshifts showing the effect of citrate-Mg^{2+} on AcnR-DNA binding.** *A*, influence of Mg^{2+} and citrate on AcnR-DNA binding, separately and in combination. A 2 nM concentration of a Cy3-labeled DNA fragment covering the promoter region of *acn* was incubated with AcnR, Mg^{2+}, and/or citrate as indicated. Only if both citrate and Mg^{2+} are added can a backshift be observed. *B*, reversibility of the citrate-Mg^{2+} effect. AcnR was incubated with DNA in binding buffer. A sample was taken (2), and the remaining complex was supplemented with Mg^{2+} and citrate. After a further 5 min, another sample was taken (3). EDTA was added, and another sample was taken after 5 min (4). *C*, influence of citrate-Mg^{2+} on mutational variants of AcnR. Arg-130 is involved in citrate binding, and the R130A variant no longer reacts to citrate-Mg^{2+}. The same amino acid exchange at another position (Arg-92 within the P pocket) does not change the behavior of AcnR in the presence of citrate-Mg^{2+}.

TABLE 2

Properties of AcnR derivatives used

Mutation	Location	Further information
pEKEx2-AcnR-STREP derivatives		
K43A	DBD	Almost complete abolishment of DNA binding
K55A	DBD	Complete abolishment of DNA binding
K104A	Dimer interface	DNA affinity close to wild-type protein
E65A	Beginning of α4	Maybe involved in signal transduction to the DNA binding domain, no effect on DNA binding
D66A	Beginning of α4	Maybe involved in signal transduction to the DNA binding domain, no effect on DNA binding
R99A	P pocket	Weaker binding to DNA
D109A	Protein surface	No effect on DNA binding
R130A	D pocket	Hydrogen-bonds to citrate, does not change its affinity to DNA in the presence of citrate-Mg^{2+}
R141A	Protein surface	No effect on DNA binding
D143A	Protein surface	No effect on DNA binding
D158A	P pocket	Weaker binding to DNA
E181A	D pocket	Binds Mg ion, does not change its affinity to DNA in the presence of citrate-Mg^{2+}
R185A	D pocket	Hydrogen-bonds to citrate, does not change its affinity to DNA in the presence of citrate-Mg^{2+}
pET-TEV-AcnR derivatives		
C23A	Within α1	No obvious difference in behavior,
R69A	P pocket	No obvious difference in behavior
M70A	P pocket	No obvious difference in behavior
M86A	P pocket	No obvious difference in behavior
R92A	P pocket	No obvious difference in behavior
W95A	P pocket	No obvious difference in behavior
R130A	D pocket	Does not change its affinity to DNA in the presence of citrate-Mg^{2+}

advance of the three-dimensional structure, but their properties can now be assessed in structural terms. A summary of these results is given in Table 2.

Mutations in the DNA-binding Region—Mutein K55A shows no binding to the *acn* promoter even at concentrations up to 770 nM, indicating either a crucial role for DNA binding or defects in folding. It is located at the beginning of α4, is equivalent to Lys-48 in TetR, and is the most conserved residue in the TetR family, forming conserved hydrogen bonds with the car-

bonyl oxygen atoms at positions 22 and 25 (positions 29 and 32 in AcnR). In addition, it is proposed to form a salt bridge with the DNA phosphate backbone. Lys-43 is not conserved, but it is located between α2 and α3 at the dimer interface and might be involved in the recognition of the specific binding sequence. Its mutation has only a minor effect on DNA binding, but it might
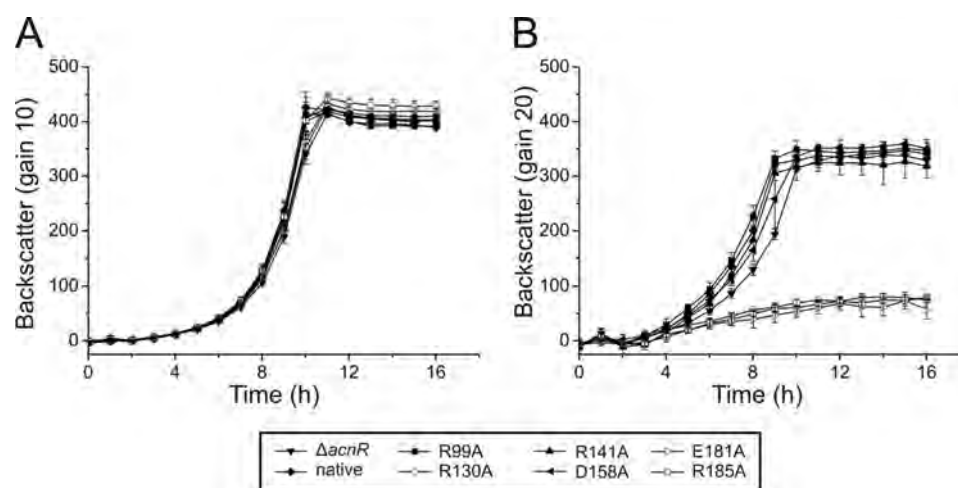
FIGURE 9. **Growth of *C. glutamicum* Δ*acnR* harboring different AcnR variants on glucose (*A*) and citrate (*B*).** After precultivation in brain-heart infusion broth and CGXII glucose medium, cells of *C. glutamicum* Δ*acnR* carrying pEKEx2 plasmids encoding the native or a mutational variant of AcnR were cultivated in CGXII minimal medium containing either 111 mM glucose (*A*) or 50 mM sodium citrate and 5 mM CaCl₂ (*B*) at 30 °C and 1200 rpm in a Biolector® system. Averages and S.D. values (*error bars*) of three biological replicates are shown.

be involved in signal transduction because it connects α6 in the LBD from one subunit with α1 in the DBD from the other subunit.

Mutations in the D Pocket—To confirm the specificity of the interaction between AcnR and citrate-Mg^{2+}, we introduced mutations in residues involved in binding of either citrate or Mg^{2+}. For muteins R130A, E181A, and R185A, the inhibition of DNA binding by citrate-Mg^{2+} is no longer observed (Fig. 8*C*; data for E181A and R185A not shown). As controls, we used variants with mutations in other domains (R95A and C26A), which behaved like the wild-type protein.

Mutations in the P Pocket—The D109A, R141A D143A, E65A, and D66A mutations had no effect on DNA binding, but an effect might be anticipated if experiments were done in the presence of a yet to be identified P ligand alone or in combination with citrate-Mg^{2+}. The mutations R99A and D158A are located in α6 and α8, respectively, and resulted in a lower affinity for DNA. Their side chains extend into the P pocket and might be involved in ligand binding.

Effect of AcnR Variants under Physiological Conditions—To test for an *in vivo* effect of the AcnR variants that are defective in citrate binding (R130A, E181A, and R185A), *C. glutamicum* Δ*acnR* was transformed with plasmid-encoded AcnR variants and cultivated in CGXII minimal medium with either glucose or citrate as carbon source (Fig. 9). On glucose, no significant growth differences between the strains were observed. In contrast, on citrate, the three strains with citrate binding-defective AcnR were no longer able to grow. All other tested AcnR variants with amino acid exchanges not affecting citrate-Mg^{2+} binding (R99A, R141A, and D158A) and wild-type AcnR did not influence growth on citrate.

Purification and Analysis of M. tuberculosis AcnR—The AcnR homologues of *C. glutamicum* and *M. tuberculosis* (Rv1474c) share a sequence identity of 53% and a similarity of 69%. Nonetheless, the MtAcnR protein showed very different properties during purification and analysis. It was not possible to overproduce MtAcnR in a soluble form in *E. coli* using the pET-TEV-MtAcnR plasmid. Several purification attempts

under denaturing conditions followed by refolding also failed. By fusing MtAcnR to the *E. coli* maltose-binding protein (MBP) lacking its signal peptide, it was possible to obtain soluble protein that could be purified by amylose affinity chromatography. The resulting fusion protein was used for EMSAs with a DNA fragment covering the promoter region of the *M. tuberculosis* aconitase gene. The band of the unbound DNA disappeared upon incubation with MBP-MtAcnR, but no distinct band of the protein-DNA complex was observed. Therefore, the MBP part of the fusion protein was cleaved off by TEV protease, which led to immediate aggregation of most of the cleaved MtAcnR. The aggregates were removed by centrifugation, and the supernatant, which contained small amounts of soluble MtAcnR in addition to uncleaved fusion protein and MBP, was used for EMSAs. This resulted in a distinct band representing the MtAcnR-DNA complex (data not shown), confirming that MtAcnR, like CgAcnR, binds to the promoter region of the *M. tuberculosis* aconitase gene.

DISCUSSION

The AcnR Fold—The structure is typical of the TetR family of transcriptional regulators with a homodimer in an Ω-shape with a DBD and a LBD. A search in SCOP (58) with the AcnR coordinates showed as main hits two known repressors belonging to the TetR family, the QacR protein (Protein Data Bank code 1JTO) and the γ-butyrolactone receptor (Protein Data Bank code 1UI5).

Binding Properties of AcnR and Effector Search—The apparent K_D for binding of AcnR to its operator in the *acn* promoter region was determined to be 7.7 nM, in the range expected for this type of repressor, and the specificity of binding was confirmed. In the search for ligands that prevent DNA binding of AcnR, citrate was always considered as a favorite candidate, because it is the substrate of aconitase and its accumulation in the cell would indicate insufficient aconitase activity. We recently showed that deletion of the *acn* gene in *C. glutamicum* strongly favors secondary mutations in the *gltA* gene encoding citrate synthase that lead to enzyme inactivation or degradation

(12). Because aconitase is the only enzyme in *C. glutamicum* known to metabolize citrate, citrate accumulation can be assumed to have toxic effects (*e.g.* by chelating divalent metal ions, such as Mg^{2+} or Fe^{2+}, or by allosteric inhibition of key metabolic enzymes). The *gltA* mutations prevent citrate formation and thus its potentially toxic effects. Citrate was strictly required for crystallization of AcnR and was bound to the D pocket in both crystal forms. Only after modifying the EMSA conditions to exclude EDTA could an inhibitory effect of citrate-Mg^{2+} on AcnR-DNA binding be shown.

In Vivo Effect of AcnR Mutations—During analysis of the *in vivo* effect of the AcnR variants that no longer reacted to citrate-Mg^{2+} in EMSA studies (R130A, E181A, and R185A), it was found that *C. glutamicum ΔacnR* strains carrying these variants are unable to grow on citrate, whereas growth on glucose was not affected. Only after more than 40 h was growth observed in the respective wells, most likely due to suppressor mutations. Aconitase is the only known enzyme of *C. glutamicum* that is able to metabolize citrate and therefore is strictly required for growth on this substrate, which can be imported by two different transport systems (50, 59). Aconitase transcription is repressed by AcnR, which is itself inhibited by the binding of citrate-Mg^{2+}. This derepression is impeded with the AcnR variants described above, which seems to completely block citrate metabolism. Aconitase deletion mutants are not able to grow in CGXII glucose medium without the addition of glutamate or glutamine (12). Because the strains carrying the citrate binding-defective AcnR variants were still able to grow in glucose medium, aconitase transcription cannot be entirely blocked. Several reasons can be envisaged for the differences in the growth behavior on glucose and citrate of the mutant strains carrying AcnR-R130A, -E181A, or -R185A. (i) During growth on glucose, but not on citrate, the postulated second effector molecule of AcnR is formed in a concentration sufficient to cause derepression of *acn*, although citrate cannot bind to AcnR anymore. This option requires that binding of this effector molecule to AcnR or its derivatives is sufficient to inhibit the interaction with the operator. It is also possible that the mutations in AcnR lead to conformational changes in such a way that the second effector molecule alone is able to inhibit AcnR-DNA complex formation. (ii) The carbon flux through aconitase is lower on glucose than on citrate, and the residual aconitase expression in the presence of the citrate binding-defective AcnR proteins is sufficient to allow this flux. On citrate, the aconitase activity is insufficient; citrate accumulates within the cells and inhibits growth, as discussed in our previous work (12). (iii) The repression by the mutated AcnR derivatives could also inhibit *acn* expression by preventing positive regulation of *acn* by other regulators, such as RamA (15). It was shown before that in a *ΔacnR* mutant, the aconitase activity is 1.7-fold higher on citrate than on glucose, in line with a transcriptional activation of *acn* during growth on citrate (8).

The D Pocket—This small pocket is positioned further away from the DBD than the canonical P pocket. It is occupied in both native structures by a citrate-Mg^{2+} moiety, which forms very specific contacts with high shape and electrostatic complementarity, including six protein-citrate hydrogen bonds plus one protein-magnesium bond, with residues contacting the

ligand being highly conserved. Subsequently, an inhibitory effect of citrate-Mg^{2+} on DNA binding was shown in EMSA studies but only in the absence of EDTA (Fig. 8*B*). Furthermore, the affinity of citrate-Mg^{2+} for AcnR is in a range that is likely to be physiologically significant, because the lack of converting enzyme leads to an increase of citrate. This strongly suggests that citrate-Mg^{2+} plays a biological role.

The Possibility of Two Ligand Binding Pockets per Protomer—We have shown that citrate-Mg^{2+} binding to the D pocket has a functional effect. This is a new site, not seen in previous TetR family receptors. However, under the conditions used, even 10 mM citrate-Mg^{2+} does not completely prevent DNA binding, and the inhibition could be overcome by using more AcnR protein (Fig. 8).

There is a second larger pocket in AcnR close to the canonical TetR ligand binding site, but we see no ligand at this site, and the only conserved residues in the AcnR subfamily in this pocket are Asp-158 and Trp-116. Nevertheless, the structural changes observed in the two protomers in crystal Form II resemble those occurring in the TetR repressor upon ligand binding, which may suggest that there is a second effector molecule that binds to the P site. One possibility would be a second ligand that influences the DNA-binding ability independently of citrate-Mg^{2+}. However, although we tested a large set of possible ligands, none inhibited DNA binding. Alternatively, there might be cross-talk between the P and the D pockets, with the putative second ligand and citrate-Mg^{2+} showing negative or positive cooperativity. Such behavior would add an additional level of complexity to the regulation of AcnR and be in line with an exceptionally tight regulation of aconitase synthesis, because it is presumed to be the only enzyme of *C. glutamicum* capable of metabolizing citrate (12); is oxygen-sensitive due to its iron-sulfur cluster (10); and is part of three important metabolic pathways, the TCA cycle, the methylcitrate cycle, and the glyoxylate shunt.

The D Pocket Is Unique to AcnR—Superposition of the AcnR DBD on those of other TetR members shows a highly conserved structure. However, the LBD shows a much lower similarity apart from the three core helices. Nevertheless, there is a resemblance in the general fold regarding the orientation and packing of the helices against one another. A clear difference between AcnR and other members is the shortening of helices 4 and 5, which appears to result in the creation of the entrance to the independent D pocket. This feature cannot only be seen in the structure but is also evident in sequence alignments where there is a deletion of seven residues compared with TetR and of up to 10 residues compared with AcrR. This deletion also occurs in other AcnRs belonging to non-*C. glutamicum* species, such as *C. diphtheriae*, suggesting that the pocket is present throughout the AcnR family.

One exception to this is the structure of EthR in complex with hexanoic acid (60) (Protein Data Bank code 1U9O), where the ligand occupies the canonical proximal site, binding between the three core helices, but stretches beyond the P pocket up between helices 4, 5, 7, and 9 to also fill a space essentially equivalent to that of the citrate-Mg^{2+} pocket in AcnR. Thus, in EthR, although the position equivalent to the AcnR citrate-Mg^{2+} pocket is also involved in ligand binding,

here it simply forms an extension of the larger P pocket. Furthermore, in EthR, helices 4 and 5 extend as far as 7 and 9 and block direct access to this pocket, leaving it to be accessed exclusively through the P pocket. In summary, most of the structures do not contain a D pocket due to the extension of helices 4 and 5, with the exception of EthR, where it acts as an extension of the canonical P pocket to accommodate the hexanoic acid.

DNA Binding and Allosteric Mechanism—The binding of TetR to DNA is proposed to depend on its inherent flexibility, whereas upon ligand binding, TetR becomes rigid and can no longer bind DNA. The first evidence in support of this was that the ligand-free structure had a longer distance between the DBD than that needed to bind two consecutive major grooves on the DNA; this distance was even bigger than in the tetracycline-bound crystal form. A mechanism was proposed where, upon binding of tetracycline-Mg^{2+} in the canonical pocket, helix $\alpha6$ unwinds and is displaced to the inside of the pocket, $\alpha4$ then acts as a pivotal point to transmit the information to the DBDs, and TetR is released from DNA. Lys-48 (Lys-55 in AcnR and conserved among all TetR members) on $\alpha4$ has been proposed to account for most of the energy of interaction with DNA. It has been supposed that other members of the family have similar mechanisms, excepting CmeR, where the affinity for DNA is lost not because of rigidification but due to disordering of the recognition helix (61).

In AcnR, the center-to-center HTH distance is about 42 Å for both crystal forms, similar to that in unliganded TetR. The differences between the two subunits in crystal Form II resemble the structural changes that occur in TetR upon binding of tetracycline-Mg^{2+}. Helix $\alpha6$ of protomer B in AcnR Form II unwinds and is displaced toward the center of the cavity. It is likely that this conformational change between the two AcnR protomers reveals biologically relevant changes upon ligand binding, similar to that in TetR, upon binding of the putative second ligand. However, the mechanism of transmission of the signal from the citrate-binding pocket to the DBD is not clear from the crystal structures because both crystal forms contain citrate-Mg^{2+} in the D pocket. This provides further support for a putative second ligand, yet to be identified, binding to the P site.

Role of AcnR in Other Members of Corynebacteriales—The AcnR protein sequence and the location of its gene downstream of an aconitase gene are highly conserved within bacteria of the order Corynebacteriales; for example, the AcnR homologue of *Mycobacterium tuberculosis* (Rv1474c) shares a sequence identity of 53%. We purified the AcnR protein from *M. tuberculosis* and demonstrated that it binds to the promoter region of the *acn* gene (Rv1475c) of this pathogenic species. This supports the view that the AcnR homologues have a similar function.

REFERENCES

1. Kinoshita, S., Udaka, S., and Shimono, M. (1957) Studies of amino acid fermentation. I. Production of L-glutamic acid by various microorganisms. *J. Gen. Appl. Microbiol.* **3,** 193–205
2. Leuchtenberger, W., Huthmacher, K., and Drauz, K. (2005) Biotechnological production of amino acids and derivatives. Current status and prospects. *Appl. Microbiol. Biotechnol.* **69,** 1–8
3. Eggeling, L., and Bott, M. (2005) *Handbook of Corynebacterium glutamicum*, CRC Press, Inc., Boca Raton, FL
4. Burkovski, A. (2008) *Corynebacteria: Genomics and Molecular Biology*, Caister Academic Press, Norfolk, UK
5. Yukawa, H., and Inui, M. (2013) *Corynebacterium glutamicum: Biology and Biotechnology*, Springer Verlag, Heidelberg
6. Bott, M. (2007) Offering surprises. TCA cycle regulation in *Corynebacterium glutamicum. Trends Microbiol.* **15,** 417–425
7. Bott, M., and Eikmanns, B. J. (2013) TCA cycle and glyoxylate shunt of *Corynebacterium glutamicum.* in *Corynebacterium glutamicum: Biology and Biotechnology* (Yukawa, H., and Inui, M., eds) pp. 281–314, Springer Verlag, Heidelberg
8. Krug, A., Wendisch, V. F., and Bott, M. (2005) Identification of AcnR, a TetR-type repressor of the aconitase gene *acn* in *Corynebacterium glutamicum. J. Biol. Chem.* **280,** 585–595
9. Beinert, H., Kennedy, M. C., and Stout, C. D. (1996) Aconitase as iron-sulfur protein, enzyme, and iron-regulatory protein. *Chem. Rev.* **96,** 2335–2374
10. Baumgart, M., and Bott, M. (2011) Biochemical characterisation of aconitase from *Corynebacterium glutamicum. J. Biotechnol.* **154,** 163–170
11. Gruer, M. J., and Guest, J. R. (1994) 2 genetically-distinct and differentially-regulated aconitases (AcnA and AcnB) in *Escherichia coli. Microbiology* **140,** 2531–2541
12. Baumgart, M., Mustafi, N., Krug, A., and Bott, M. (2011) Deletion of the aconitase gene in *Corynebacterium glutamicum* causes a strong selection pressure for secondary mutations inactivating citrate synthase. *J. Bacteriol.* **193,** 6864–6873
13. Wendisch, V. F., de Graaf, A. A., Sahm, H., and Eikmanns, B. J. (2000) Quantitative determination of metabolic fluxes during coutilization of two carbon sources. Comparative analyses with *Corynebacterium glutamicum* during growth on acetate and/or glucose. *J. Bacteriol.* **182,** 3088–3096
14. Wennerhold, J., Krug, A., and Bott, M. (2005) The AraC-type regulator RipA represses aconitase and other iron proteins from *Corynebacterium* under iron limitation and is itself repressed by DtxR. *J. Biol. Chem.* **280,** 40500–40508
15. Emer, D., Krug, A., Eikmanns, B. J., and Bott, M. (2009) Complex expression control of the *Corynebacterium glutamicum* aconitase gene. Identification of RamA as a third transcriptional regulator besides AcnR and RipA. *J. Biotechnol.* **140,** 92–98
16. Han, S. O., Inui, M., and Yukawa, H. (2008) Effect of carbon source availability and growth phase on expression of *Corynebacterium glutamicum* genes involved in the tricarboxylic acid cycle and glyoxylate bypass. *Microbiology* **154,** 3073–3083
17. Frunzke, J., and Bott, M. (2008) Regulation of iron homeostasis in *Corynebacterium glutamicum.* in *Corynebacteria: Genomics and Molecular Biology* (Burkovski, A., ed) pp. 241–266, Caister Academic Press, Norfolk, UK
18. Cramer, A., Gerstmeir, R., Schaffer, S., Bott, M., and Eikmanns, B. J. (2006) Identification of RamA, a novel LuxR-type transcriptional regulator of genes involved in acetate metabolism of *Corynebacterium glutamicum. J. Bacteriol.* **188,** 2554–2567
19. Kohl, T. A., and Tauch, A. (2009) The GlxR regulon of the amino acid producer *Corynebacterium glutamicum*. Detection of the corynebacterial core regulon and integration into the transcriptional regulatory network model. *J. Biotechnol.* **143,** 239–246
20. Toyoda, K., Teramoto, H., Inui, M., and Yukawa, H. (2011) Genome-wide identification of *in vivo* binding sites of GlxR, a cyclic AMP receptor protein-type regulator in *Corynebacterium glutamicum. J. Bacteriol.* **193,** 4123–4133
21. Ramos, J. L., Martínez-Bueno, M., Molina-Henares, A. J., Terán, W., Wa-

tanabe, K., Zhang, X., Gallegos, M. T., Brennan, R., and Tobes, R. (2005) The TetR family of transcriptional repressors. *Microbiol. Mol. Biol. Rev.* **69,** 326–356

22. Yu, Z., Reichheld, S. E., Savchenko, A., Parkinson, J., and Davidson, A. R. (2010) A comprehensive analysis of structural and sequence conservation in the TetR family transcriptional regulators. *J. Mol. Biol.* **400,** 847–864

23. Orth, P., Saenger, W., and Hinrichs, W. (1999) Tetracycline-chelated Mg^{2+} ion initiates helix unwinding in Tet repressor induction. *Biochemistry* **38,** 191–198

24. Orth, P., Schnappinger, D., Hillen, W., Saenger, W., and Hinrichs, W. (2000) Structural basis of gene regulation by the tetracycline inducible Tet repressor-operator system. *Nat. Struct. Biol.* **7,** 215–219

25. Schumacher, M. A., Miller, M. C., Grkovic, S., Brown, M. H., Skurray, R. A., and Brennan, R. G. (2001) Structural mechanisms of QacR induction and multidrug recognition. *Science* **294,** 2158–2163

26. Schumacher, M. A., Miller, M. C., Grkovic, S., Brown, M. H., Skurray, R. A., and Brennan, R. G. (2002) Structural basis for cooperative DNA binding by two dimers of the multidrug-binding protein QacR. *EMBO J.* **21,** 1210–1218; Correction (2002) *EMBO J.* **21,** 2301

27. Itou, H., Okada, U., Suzuki, H., Yao, M., Wachi, M., Watanabe, N., and Tanaka, I. (2005) The CGL2612 protein from *Corynebacterium glutamicum* is a drug resistance-related transcriptional repressor. Structural and functional analysis of a newly identified transcription factor from genomic DNA analysis. *J. Biol. Chem.* **280,** 38711–38719

28. Itou, H., Watanabe, N., Yao, M., Shirakihara, Y., and Tanaka, I. (2010) Crystal structures of the multidrug binding repressor *Corynebacterium glutamicum* CgmR in complex with inducers and with an operator. *J. Mol. Biol.* **403,** 174–184

29. Le, T. B., Schumacher, M. A., Lawson, D. M., Brennan, R. G., and Buttner, M. J. (2011) The crystal structure of the TetR family transcriptional repressor SimR bound to DNA and the role of a flexible N-terminal extension in minor groove binding. *Nucleic Acids Res.* **39,** 9433–9447

30. Le, T. B., Stevenson, C. E., Fiedler, H.-P., Maxwell, A., Lawson, D. M., and Buttner, M. J. (2011) Structures of the TetR-like simocyclinone efflux pump repressor, SimR, and the mechanism of ligand-mediated derepression. *J. Mol. Biol.* **408,** 40–56

31. García-Nafría, J., Baumgart, M., Bott, M., Wilkinson, A. J., and Wilson, K. S. (2010) The *Corynebacterium glutamicum* aconitase repressor. Scratching around for crystals. *Acta Crystallogr. Sect. F Struct. Biol. Cryst. Commun.* **66,** 1074–1077

32. Sambrook, J., Fritsch, E. F., and Maniatis, T. (1989) *Molecular cloning: A Laboratory Manual*, Cold Spring Harbor Laboratory, Cold Spring Harbor, NY

33. Eikmanns, B. J., Thum-Schmitz, N., Eggeling, L., Lüdtke, K. U., and Sahm, H. (1994) Nucleotide-sequence, expression and transcriptional analysis of the *Corynebacterium glutamicum gltA* gene encoding citrate synthase. *Microbiology* **140,** 1817–1828

34. Hanahan, D. (1983) Studies on transformation of *Escherichia coli* with plasmids. *J. Mol. Biol.* **166,** 557–580

35. Schmidt, T. G., and Skerra, A. (2007) The Strep-tag system for one-step purification and high-affinity detection or capturing of proteins. *Nat. Protoc.* **2,** 1528–1535

36. Niebisch, A., Kabus, A., Schultz, C., Weil, B., and Bott, M. (2006) Corynebacterial protein kinase G controls 2-oxoglutarate dehydrogenase activity via the phosphorylation status of the OdhI protein. *J. Biol. Chem.* **281,** 12300–12307

37. Leslie, A. G. (2006) The integration of macromolecular diffraction data. *Acta Crystallogr. D Biol. Crystallogr.* **62,** 48–57

38. Battye, T. G., Kontogiannis, L., Johnson, O., Powell, H. R., and Leslie, A. G. (2011) iMOSFLM. A new graphical interface for diffraction-image processing with MOSFLM. *Acta Crystallogr. D Biol. Crystallogr.* **67,** 271–281

39. Evans, P. (2006) Scaling and assessment of data quality. *Acta Crystallogr. D Biol. Crystallogr.* **62,** 72–82

40. Winn, M. D., Ballard, C. C., Cowtan, K. D., Dodson, E. J., Emsley, P., Evans, P. R., Keegan, R. M., Krissinel, E. B., Leslie, A. G., McCoy, A., McNicholas, S. J., Murshudov, G. N., Pannu, N. S., Potterton, E. A., Powell, H. R., Read, R. J., Vagin, A., and Wilson, K. S. (2011) Overview of the CCP4 suite and current developments. *Acta Crystallogr. D Biol. Crystallogr.* **67,** 235–242

41. Otwinowski, Z., and Minor, W. (1997) Processing of X-ray diffraction data collected in oscillation mode. *Methods Enzymol.* **276,** 307–326

42. Sheldrick, G. M. (2010) Experimental phasing with SHELXC/D/E. Combining chain tracing with density modification. *Acta Crystallogr. D Biol. Crystallogr.* **66,** 479–485

43. Cowtan, K. (2006) The Buccaneer software for automated model building. 1. Tracing protein chains. *Acta Crystallogr. D Biol. Crystallogr.* **62,** 1002–1011

44. Emsley, P., and Cowtan, K. (2004) Coot: model-building tools for molecular graphics. *Acta Crystallogr. D Biol. Crystallogr.* **60,** 2126–2132

45. Murshudov, G. N., Skubák, P., Lebedev, A. A., Pannu, N. S., Steiner, R. A., Nicholls, R. A., Winn, M. D., Long, F., and Vagin, A. A. (2011) REFMAC5 for the refinement of macromolecular crystal structures. *Acta Crystallogr. D Biol. Crystallogr.* **67,** 355–367

46. McCoy, A. J., Grosse-Kunstleve, R. W., Adams, P. D., Winn, M. D., Storoni, L. C., and Read, R. J. (2007) Phaser crystallographic software. *J. Appl. Crystallogr.* **40,** 658–674

47. Davis, I. W., Murray, L. W., Richardson, J. S., and Richardson, D. C. (2004) MolProbity. Structure validation and all-atom contact analysis for nucleic acids and their complexes. *Nucleic Acids Res.* **32,** W615–W619

48. van der Rest, M. E., Lange, C., and Molenaar, D. (1999) A heat shock following electroporation induces highly efficient transformation of *Corynebacterium glutamicum* with xenogeneic plasmid DNA. *Appl. Microbiol. Biotechnol.* **52,** 541–545

49. Keilhauer, C., Eggeling, L., and Sahm, H. (1993) Isoleucine synthesis in *Corynebacterium glutamicum*. Molecular analysis of the *ilvB-ilvN-ilvC* operon. *J. Bacteriol.* **175,** 5595–5603

50. Brocker, M., Schaffer, S., Mack, C., and Bott, M. (2009) Citrate utilization by *Corynebacterium glutamicum* is controlled by the CitAB two-component system through positive regulation of the citrate transport genes *citH* and *tctCBA*. *J. Bacteriol.* **191,** 3869–3880

51. Aleksandrov, A., Schuldt, L., Hinrichs, W., and Simonson, T. (2008) Tet repressor induction by tetracycline. A molecular dynamics, continuum electrostatics, and crystallographic study. *J. Mol. Biol.* **378,** 898–912

52. Orth, P., Cordes, F., Schnappinger, D., Hillen, W., Saenger, W., and Hinrichs, W. (1998) Conformational changes of the Tet repressor induced by tetracycline trapping. *J. Mol. Biol.* **279,** 439–447

53. Krissinel, E., and Henrick, K. (2007) Inference of macromolecular assemblies from crystalline state. *J. Mol. Biol.* **372,** 774–797

54. Krissinel, E., and Henrick, K. (2004) Secondary-structure matching (SSM), a new tool for fast protein structure alignment in three dimensions. *Acta Crystallogr. D Biol. Crystallogr.* **60,** 2256–2268

55. Dundas, J., Ouyang, Z., Tseng, J., Binkowski, A., Turpaz, Y., and Liang, J. (2006) CASTp. Computed atlas of surface topography of proteins with structural and topographical mapping of functionally annotated residues. *Nucleic Acids Res.* **34,** W116–W118

56. Jo, S., Vargyas, M., Vasko-Szedlar, J., Roux, B., and Im, W. (2008) PBEQ-Solver for online visualization of electrostatic potential of biomolecules. *Nucleic Acids Res.* **36,** W270–W275

57. Bennett, B. D., Kimball, E. H., Gao, M., Osterhout, R., Van Dien, S. J., and Rabinowitz, J. D. (2009) Absolute metabolite concentrations and implied enzyme active site occupancy in *Escherichia coli*. *Nat. Chem. Biol.* **5,** 593–599

58. Murzin, A. G., Brenner, S. E., Hubbard, T., and Chothia, C. (1995) SCOP. A structural classification of proteins database for the investigation of sequences and structures. *J. Mol. Biol.* **247,** 536–540

59. Polen, T., Schluesener, D., Poetsch, A., Bott, M., and Wendisch, V. F. (2007) Characterization of citrate utilization in *Corynebacterium glutamicum* by transcriptome and proteome analysis. *FEMS Microbiol. Lett.* **273,** 109–119

60. Frénois, F., Engohang-Ndong, J., Locht, C., Baulard, A. R., and Villeret, V. (2004) Structure of EthR in a ligand bound conformation reveals therapeutic perspectives against tuberculosis. *Mol. Cell* **16,** 301–307

61. Gu, R., Su, C. C., Shi, F., Li, M., McDermott, G., Zhang, Q., and Yu, E. W. (2007) Crystal structure of the transcriptional regulator CmeR from *Campylobacter jejuni*. *J. Mol. Biol.* **372,** 583–593

62. McNicholas, S., Potterton, E., Wilson, K. S., and Noble, M. E. (2011) Presenting your structures. The CCP4mg molecular-graphics software. *Acta Crystallogr. D Biol. Crystallogr.* **67,** 386–394

Crystal and Solution Studies Reveal That the Transcriptional Regulator AcnR of *Corynebacterium glutamicum* Is Regulated by Citrate-Mg^{2+} Binding to a Non-canonical Pocket

Javier García-Nafría, Meike Baumgart, Johan P. Turkenburg, Anthony J. Wilkinson, Michael Bott and Keith S. Wilson

Access the most updated version of this article at doi: 10.1074/jbc.M113.462440

Alerts:
- When this article is cited
- When a correction for this article is posted

Click here to choose from all of JBC's e-mail alerts

Supplemental material:
http://www.jbc.org/content/suppl/2013/04/15/M113.462440.DC1

This article cites 56 references, 13 of which can be accessed free at
http://www.jbc.org/content/288/22/15800.full.html#ref-list-1